TABLE 1 Simulated Peak Value of the Quality Factor Based on the Present DCM Model (S-DCM) Compared to the Measurement

N	Q_{peak} Measure	Q_{peak} [S-DCM]	Q_{peak} [%] Deviation	f_{SR} [GHz] Measure	f_{SR} [GHz] (S-DCM)	f_{SR} [%] Deviation	Q RMS [%] 0.1–10 GHz
2.5	1.707	12.316	5.3	18.5	20.10	8.6	1.2
3.5	9.3962	9.9274	5.6	11.58	11.79	1.8	2.2
4.5	8.4327	8.8223	4.6	7.65	7.80	1.9	3.5
5.5	7.8822	7.7853	1.2	5.40	5.24	3.0	5
6.5	7.1194	6.8578	3.7	4.1408	3.7367	9.8	9.7

The deviations are about 4% on average for all the five inductors of different number of turns. The simulated and measured self-resonance frequency f_{SR} is also shown and exhibit 5% deviations in average. For the 5.5 turn inductor, the nonscalable DCM model of [14] yields a deviation for f_{SR} of more than 15% compared to 3% of the present value. The RMS deviation for simulated Q (S-DCM) between 0.1 and 10 GHz is 4% in average.

The peak Q value is listed in Table 1. The deviation of simulation from measurement is within 4% in average for all the five inductors. Another major parameter in inductor simulation is the self-resonance frequency f_{SR}. As can be seen in Table 1, the simulated f_{SR} exhibits 5% deviation from measurement based on the present model. As a comparison, the deviation for the 5.5-turn inductor based on the non-scalable DCM model is more than 15%.

5. CONCLUSION

In summary, we have developed a scalable distributed-capacitance model for the coupling capacitance between metal lines in silicon on-chip spiral inductors. As compared to the previous DCM model, the current approach yields scalable characteristics for the coupling capacitance for a series of inductors with different number of turns. The current formulations can provide simulations in good agreement with measurement for the inductor quality factor Q with an average root-mean-square deviation of less than 4%, for frequency between 0.1 and 10 GHz, and for inductors of different number of turns ranging from 2.5 to 6.5. The close match between simulation and measurement demonstrates the validity of the present approach.

ACKNOWLEDGMENTS

F. Huang acknowledges the support of grant no. 20040286022 and NSF no. 60476012. N. Jiang acknowledges support by the National Natural Science Foundation of China under grant no. 90307007.

REFERENCES

1. K.B. Ashby, I.A. Koullias, W.C. Finley, J.J. Bastek, and S. Moinian, High-Q inductors for wireless applications in a complementary silicon bipolar process, IEEE J Solid-State Circ 31 (1996), 4–9.
2. D.K. Shaffer and T.H. Lee, A 1.5-V 1.5-GHz CMOS low-noise amplifier, IEEE J Solid-State Circ 32 (1997), 745–759.
3. Y.-C. Ho, K.-H. Kim, B.A. Floyd, C. Wann, Y. Taur, U. Lagnado, and K.K. O, 4- and 13-GHz tuned amplifiers implemented in a 0.1-μm CMOS technology on SOI, SOS, and bulk substrates, IEEE J Solid-State Circ 33 (1998), 2066–2073.
4. A. Hajimiro and T.H. Lee, Design issues in CMOS differential LC oscillators, IEEE J Solid-State Circ 34 (1999), 717–724.
5. J.R. Long and M.A. Copeland, The modeling, characterization, and design of monolithic inductors for silicon RFICs, IEEE J Solid-State Circ 32 (1997), 357–368.
6. A.M. Niknejad and R.G. Meyer, Design, simulation, and applications of inductors and transformers for Si RF ICs, Kluwer, Boston, MA, 2000.
7. C.P. Yue, C. Ryu, J. Lau, T.H. Lee, and S.S. Wong, A physical model for planar spiral inductors on silicon, IEEE IEDM Dig (1996), 155–158.
8. A. Niknejad and R. Meyer, Analysis, design and optimization of spiral inductors and transformers for Si RF ICs, IEEE J Solid-State Circ 33 (1998), 470–1481.
9. A.C. Watson, D. Melendy, P. Francis, K. Hwang, and A. Weisshaar, A comprehensive compact-modeling methodology for spiral inductors in silicon-based RFICs, IEEE Trans MTT 52 (2004), 849–857.
10. B.-L. Ooi, D.-X. Xu, P.-S. Kooi, and F.-J. Lin, An improved prediction of series resistance in spiral inductor modeling with eddy-current effect, IEEE Trans MTT 50 (2002), 2202–2204.
11. Y. Cao, R.A. Groves, X. Huang, N.D. Zamdmer, J.-O. Plouchart, R.A. Wachnik, T.J. King, and C.M. Hu, Frequency-independent equivalent circuit model for on-chip spiral inductors, IEEE J Solid-State Circ 38 (2003), 419–426.
12. C. Wu, C. Tang, and S. Liu, Analysis of on-chip spiral inductors using the distributed capacitance model, IEEE J Solid-State Circ 38 (2003), 1040–1044.
13. F.Y. Huang, N. Jiang, and E.L. Bian, Modeling of single-π equivalent circuit for on-chip spiral inductors, Solid-State Electron 49 (2005), 473–478.
14. F.Y. Huang, N. Jiang, and E.L. Bian, Characteristic-function approach to parameter extraction for asymmetric equivalent circuit of on-chip spiral inductors, IEEE Trans MTT (2005).

SRR LOADED WAVEGUIDE BAND REJECTION FILTER WITH ADJUSTABLE BANDWIDTH

B. Jitha, C. S. Nimisha, C. K. Aanandan, P. Mohanan, and K. Vasudevan
Centre for Research in Electromagnetics and Antennas
Department of Electronics
Cochin University of Science and Technology
Cochin 682022, India

Received 9 January 2006

ABSTRACT: *The use of a split-ring resonator (SRR)-loaded waveguide for the design of a band-rejection filter with adjustable bandwidth is reported. The width of the stopband can be adjusted by suitably positioning the SRR array in the waveguide. The rejection band can be made very narrow by placing the array at the electric-field minimum. The stopband attenuation depends on the number of unit cells in the array.* © 2006 Wiley Periodicals, Inc. Microwave Opt Technol Lett 48: 1427–1429, 2006; Published online in Wiley InterScience (www.interscience.wiley.com). DOI 10.1002/mop.21641

Key words: *waveguide band reject filter; split-ring resonator; metamaterials*

INTRODUCTION

Propagation of electromagnetic waves in metamaterials has been a topic of intensive study in the last few years [1–4]. These materials, which exhibit negative values of permeability and permittiv-

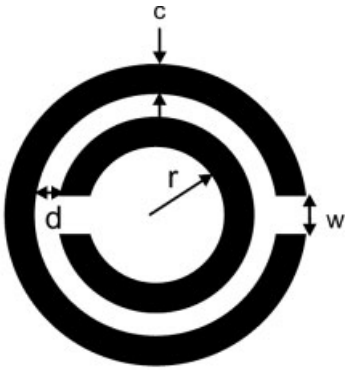

Figure 1 Unit cell of SRR array ($r = 1.6$ mm, $d = 0.2$ mm, $c = 0.9$ mm, $w = 0.2$ mm)

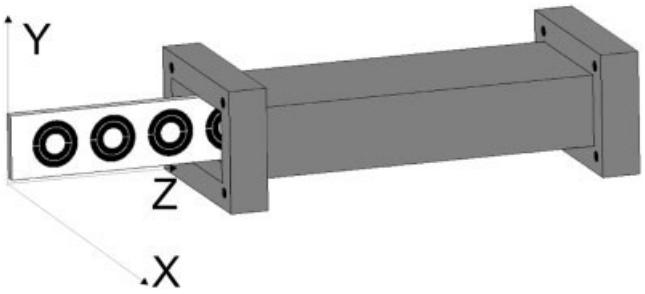

Figure 2 X-band waveguide loaded with an SRR array

ity, have received much attention due to their interesting characteristics and compact size. Structures like split-ring resonators (SRRs) and complementary split-ring resonators (CSRRs) have been proposed to develop structures which filter certain frequency bands or suppress spurious harmonics [5–7].

When a time-harmonic magnetic field is applied along the ring axis, an electromotive force appears around the SRRs. Since the electrical size of the SRR can be considered small, the induced current lines pass from one ring to the other through the capacitive gap between them in the form of field-displacement current lines. Magnetic resonance is induced by the split at the rings and by the gap between inner and outer rings. The whole device behaves as an LC circuit [2]. Geometrical parameters such as splitting width, gapping between the rings, and the metal width affect the resonant frequency.

The transmission characteristics of an SRR array inserted in a waveguide has also been investigated [8]. It was observed that the signal propagation is inhibited in the small frequency band in the waveguide passband. This has been interpreted due to the periodic medium exhibiting a negative permeability near the resonant frequency of the SRR. In this paper, we propose the use of an SRR array for the design of a waveguide band-rejection filter with adjustable band width. A single layer of an edge-coupled split-ring resonator (EC-SRR) etched on a dielectric is used for this purpose, whose position with respect to the waveguide axis determines the width of the stop band. Waveguide filters are used at high frequencies where very low insertion loss and high power handling is the requirement. They find applications in the field of avionics, satellite communication, and so forth.

DESIGN OF SRR ARRAY

The SRR array is fabricated on a single-sided FR4 substrate with dielectric constant $\varepsilon_r = 4.36$ and thickness $h = 1.6$ mm using the photolithographic technique. A unit cell of the array having a resonance in the X-band is shown in Figure 1.

SRR arrays with varying number of unit cells (N) are fabricated on single-sided FR4 strips with a period equal to 10 mm. The array is inserted parallel to the z-axis at the center of the waveguide, as shown in Figure 2.

EXPERIMENTAL AND SIMULATED RESULTS

The X-band waveguide is excited in the TE_{10} mode with two coaxial-to-rectangular waveguide transitions as input and output. An HP 8510C Network Analyzer is used to measure the transmission coefficient $|S_{21}|$. An absorption dip is observed in the waveguide pass band at around 7.8 GHz. The experiment is repeated using arrays with different number of unit cells (N). It is found that the attenuation is increasing with the number of unit cells, as shown in Figure 3. With $N = 12$, the received power level reaches the noise floor of the measuring instrument.

Now, the SRR array with $N = 12$ is moved along the broadside (x-axis) of the waveguide and the transmission characteristics are studied with the distance from the narrow wall. The width of the stopband varies with the distance x of the SRR array along the x-direction. The stopband is very narrow when the strip is near the waveguide wall and reaches a maximum value when the structure is placed at the center of the waveguide, as is evident from Figures 4 and 5. The simulated results are also shown for comparison. Here, $x = 0$ corresponds to the rings in contact with the narrow wall of the waveguide.

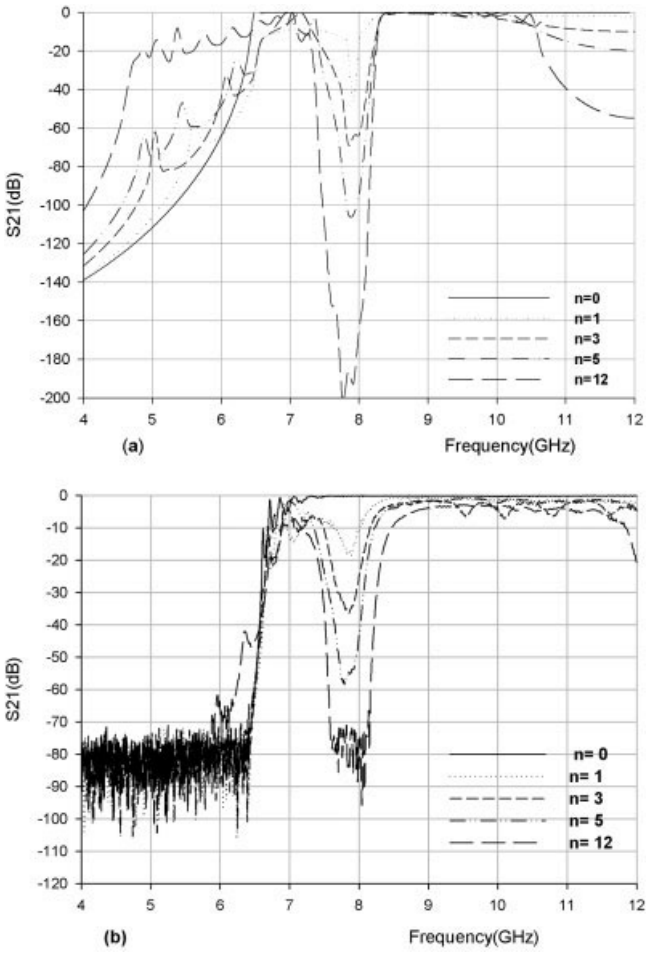

Figure 3 (a) Simulated and (b) measured transmission characteristics of the waveguide loaded with an SRR having different number of unit cells

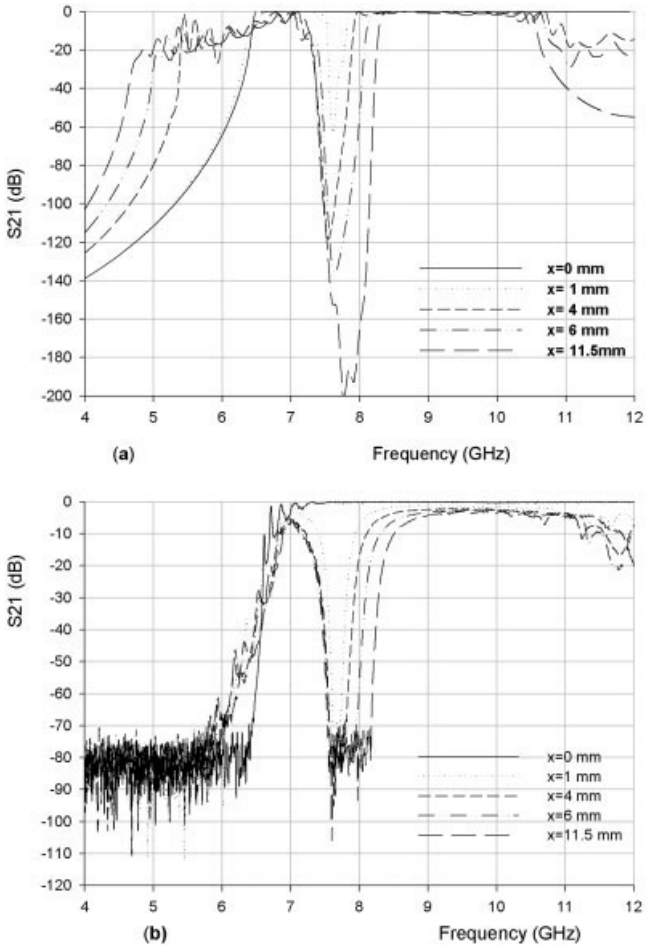

Figure 4 (a) Simulated and (b) measured transmission characteristics of the waveguide loaded with an SRR array at different positions x along the x-axis

CONCLUSIONS

Construction of waveguide band reject filter at the X-band by loading a split-ring resonator (SRR) array has been reported. The width of the rejection band can be controlled by adjusting the position of the array inside the waveguide.

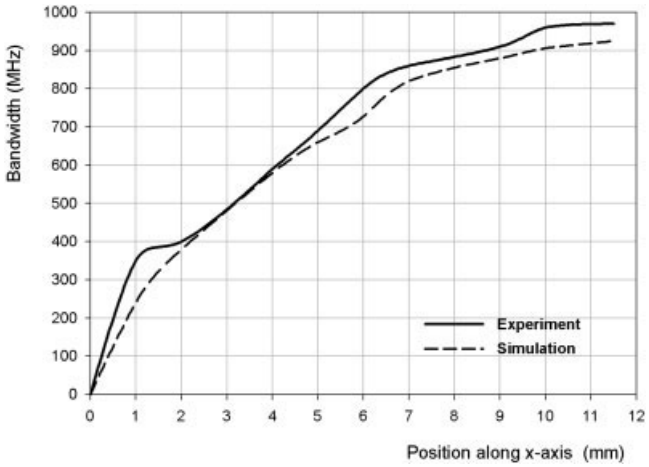

Figure 5 Variation in bandwidth vs. position of the SRR array

REFERENCES

1. D.R. Smith, W.J. Padilla, D.C. Vier, S.C. Nermat-Nasser, and S. Schultz, Composite medium with simultaneously negative permeability and permittivity, Phys Rev Lett 84 (2000), 4184–4187.
2. V. Radisic, Y. Qian, R. Coccioli, and T. Itoh, Novel 2D photonic band gap structures for microstrip lines, IEEE Microwave Guided Wave Lett 10 (1998), 69–71.
3. R. Marques, F. Mesa, J. Martel, and F. Medina, Comparative analysis of edge- and broadside coupled split ring resonators for metamaterial design-theory and experiment, IEEE Trans Antennas Propagat 51 (2003), 2572–2581.
4. J. Estaban, C. Camacho Penalosa, J.E. Page, T.M. Martin-Guerrero, and E. Marquez Segura, Simulation of negative permittivity and negative permeability by means of evanescent waveguide modes—Theory and Experiment, IEEE Trans Microwave Theory Tech 53 (2005), 1506–1514.
5. J.B. Pendry, A.J. Holden, D.J. Robbins, and W.J. Stewart, Magnetism from conductors and enhanced nonlinear phenomena, IEEE Trans Microwave Theory Tech 47 (1999), 2075–2084.
6. F. Falcone, T. Lopetegi, J.D. Baena, R. Marques, F. Martin, and M. Sorolla, Effective negative-ε stopband microstrip lines based on complementary split-ring resonators, IEEE Microwave Wireless Compon Lett 14 (2004), 280–282.
7. J.D. Baena, J. Bonache, F. Martin, R. Marques, F. Falcone, T. Lopetegi, M.A.G. Laso, J. Garcia Garcia, I. Gil, M. Flores Portillo, and M. Sorolla, Equivalent-circuit models for split-ring resonators and complementary split-ring resonators coupled to planar transmission lines, IEEE Trans Microwave Theory Tech 53 (2005), 1451–1461.
8. S. Hrabar, J. Bartolic, and Z. Sipus, Waveguide miniaturization using uniaxial negative permeability metamaterial, IEEE Trans Antennas Propagat 53 (2005), 110–119.

A DUAL-LAYERED WIDEBAND MICROSTRIP REFLECTARRAY ANTENNA WITH VARIABLE POLARIZATION

Zhi-Hang Wu, Wen-Xun Zhang, Zhen-Guo Liu, and Wei Shen
State Key Laboratory of Millimeter Waves
Southeast University
Nanjing, 210096, China

Received 9 January 2006

ABSTRACT: *This paper presents a new kind of microstrip reflectarray antenna those polarization could be reconfigurable among all polarization states instead of some fixed states for dual- or multipolarized antenna. The mechanism for polarized variability is so simple that only mechanical rotation is needed. The complete theoretical analysis is given as well as a specific design sample to verify this method. At designed frequency of 10 GHz and in case of circularly polarized (CP) radiation, experimental results in agreement with simulated ones exhibit −26-dB cross-polar level (CPL), −13-dB side-lobe level, 13.5° half-power beamwidth, and 17.3-dBi gain corresponding to about 40% aperture efficiency. It also possesses 8% bandwidth from 9.5 to 10.3 GHz for CPL less than −15 dB.* © 2006 Wiley Periodicals, Inc. Microwave Opt Technol Lett 48: 1429–1432, 2006; Published online in Wiley InterScience (www.interscience.wiley.com). DOI 10.1002/mop.21640

Key words: *reflectarray; polarization variable antenna; polarization reconfigurable antenna; wideband; high-gain*

1. INTRODUCTION

Interest in the study of the microstrip reflectarray has been greatly kindled in the past decade, because of its advantages: low-profile